Materials and Structures (2013) 46:345–360
DOI 10.1617/s11527-012-9905-3

ORIGINAL ARTICLE

Effective joining method for pseudo-ductile permanent formwork

Qingxu Jin · Christopher K. Y. Leung · Changli Yu

Received: 26 January 2012 / Accepted: 25 June 2012 / Published online: 11 July 2012

Abstract A novel joining method for permanent formwork, involving the embedment of GFRP in high-strength fiber reinforced cementitious composites (HSFRCC), is proposed. Direct pull-out test is carried out to investigate the bonding capacity between the HSFRCC and GFRP reinforcement. From the experimental data, interfacial parameters are extracted for calculating the required embedded length of GFRP bars to ensure sufficient bonding capacity. According to the test results, the required embedded length of GFRP bars is obtained and the joint width thus can be determined. To further verify the joining method, beam members made with joined and monolithic PDCC formwork are prepared and tested under four point bending. The comparison indicates only about 5 % difference between the load capacities in the two cases. Besides, the worse scenario in the test that the joint was placed at the location with the maximum moment would rarely happen in practice.

Keywords Joining method · Permanent formwork · Debonding · Pseudo-ductile cementitious composites · Durability · High-strength fiber reinforced cementitious composites

Q. Jin (✉) · C. K. Y. Leung · C. Yu
Department of Civil and Environmental Engineering of HKUST, HKSAR, China
e-mail: wildbiller@gmail.com

1 Introduction

Due to deterioration problems with many existing concrete structures, durability has become a major concern for new constructions. For reinforced concrete structures, steel corrosion is a major cause of their degradation. In fact, steel rusting should occur at a negligible rate in the alkaline environment inside concrete, as the iron oxide formed under high pH condition is very stable and can effectively protect the underlying material from corrosion. However, when chloride ions (from sea spray in coastal regions or deicing salt in cold regions) or carbon dioxide penetrate through the concrete cover to reach the steel, the protective layer will break down. Continuous rusting together with water absorption and expansion of the rust generate internal stresses that lead to cracking and spalling of the concrete cover [1]. Once major cracking or spalling occurs, penetration of corrosion agents is expedited and the degradation rate is greatly increased. Therefore, the durability of concrete structure is often governed by concrete cover since it is the main protection for steel bar being exposed to the outside environment. To delay the penetration of water, chlorides and carbon dioxide, the concrete cover can be designed with a low water/cement ratio and pozzolans can be added to reduce capillary porosity in the hardened material. This can produce concrete with low water permeability and chloride diffusivity when new. However, over the lifetime of the structure, loading, shrinkage and/or

thermal effects will lead to the formation of surface cracks that provide paths for the penetration of water and corrosive agent. While cracking is almost unavoidable in practice, if crack openings are sufficiently small (<50 μm), the effect of cracks on both water permeability and chloride diffusivity can be minimal [21, 22]. Therefore, the long-term durability can be significantly improved if a material exhibiting fine cracks with controlled opening is employed to construct concrete structures.

Pseudo-ductile cementitious composites (PDCC), a new generation of fiber reinforced composites developed based on fracture mechanics concepts and with help of micromechanical models [9, 10, 11], can significantly enhance the crack resistance of concrete because of its strain-hardening behavior with excellent crack control capability. In PDCC, the increase in load after first cracking allows the uniform formation of closely-spaced multiple cracks along the length of the specimen, with the opening of each crack limited to a very small value (which is often below 50 μm). However, the cost of PDCC is several times that of normal concrete. To make its practical application economically feasible, a feasible approach is to apply it strategically at locations critical to durability, which is the concrete cover for the steel reinforcement. The use of PDCC to fabricate permanent formwork has been used in Japan for tunnel lining [16] and bridge decks [24], while the permanent formwork made with conventional concrete and glass fiber textile reinforcement have been developed in Germany [3]. Permanent formwork made up by PDCC with embedded glass fiber reinforced plastics (GFRP) rods has been developed by Leung and Cao [8] and further studied in Yu et al. [26]. To make concrete members, the formwork is fabricated first and concrete is cast subsequently cast. According to Leung and Cao [8], transverse grooves on the formwork surface can effectively improve the bonding between the formwork element and the concrete. Also, under bending, major cracks in the cast concrete can turn into multiple fine cracks inside the PDCC. Based on the test results and design calculations, the GFRP/PDCC formwork is found suitable for building the deck slab of a 4 m wide footbridge, by the direct casting of concrete (with no additional steel reinforcements). The feasibility of using GFRP/PDCC formwork in structures under aggressive environment to eliminate the steel corrosion problem is hence demonstrated. In Yu et al. [26], beams made with rectangular formwork (placed at the bottom surface) and channel-shaped formwork (which will provide PDCC cover at the bottom and sides) were compared. In comparison to slab members, the effect of shear is much more significant in beams, and interfacial debonding of the formwork is easier to occur. It is found that the use of channel-shaped formwork can be effective in preventing or delaying debonding failure.

While relatively short members (such as the lateral spanning deck for a footbridge) can be made with a single piece of formwork element, longer members require the use of a large formwork made by the in situ joining of prefabricated formwork elements. The design of an effective joining method that allows proper transfer of loading between adjacent elements is hence a critical research issue. For the sake of construction efficiency, the joint details should also be as simple as possible and the width of the joint should be small. The latter is particular important for construction in the cold region, where the joint may have to be heated to facilitate strength development. A short joint will then significantly reduce the energy required. The development of a simple and short joint for precast concrete beam/slabs has been studied by Jensen et al. [7] and Shioya et al. [19]. In these studies, the following joining method is proposed. Two precast members with steel reinforcements extending from their ends are placed close to one another, with the extended steel bars in the joint region. High strength fiber reinforced cementitious materials (HSFRCC) is then cast to form the joint. Testing results show that the bond between HSFRCC and steel is so high that sufficient bond capacity (for steel yielding to occur) can be achieved with the use of straight steel bars and a very short joint. In Ma and Dietz [14], with the application of superplasticizer, HSFRCC with self-compacting behavior can be achieved, it will greatly stimulate the use of HSFRCC for the short joint since the compaction is not required.

In this work, a similar joining method is proposed and studied. GFRP bars from the formwork elements are extended into the joint region where HSFRCC will be cast (Fig. 1). In the literature, different kinds of high strength cementitious composites have been developed by various investigators [2, 6, 17, 18, 27]. To obtain high strength, a low W/B ratio is normally employed, together with the use of pozzolans. With the addition of steel fibers, HSFRCC can exhibit a

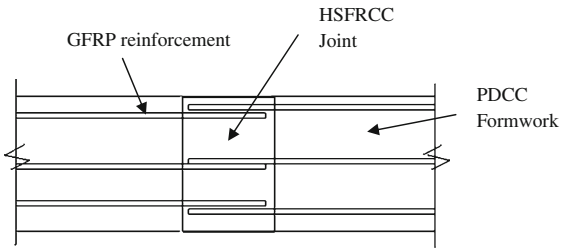

Fig. 1 GFRP grip

certain degree of strain hardening in tension as well [6, 15]. Superplasticizers are often added to improve the workability or to make the composite self-compacting. In this paper, the high-strength fiber reinforced cementitious composites (HSFRCC) developed by Cheung and Leung [6] will be employed.

This paper will focus on the joining of GFRP/PDCC permanent formwork. To determine the required width of the joint, which is governed by the bond capacity, the interfacial parameters between HSFRCC and GFRP rebar need to be obtained. These parameters can be back calculated from the load versus displacement curve of a direct pull-out test with the help of a theoretical model. Once the parameters are obtained, the bond capacity can be calculated for an arbitrary combination of the size and length of GFRP rebar. Beams with both monolithic formwork and joined formwork (with proper joint length according to the model) are then prepared and tested to verify the joining method.

2 Experimental program on bond capacity

2.1 Sample design and preparation

To study the bond behavior between GFRP and HSFRCC, the pull-out test is employed. The testing principle is very simple—an embedded rod inside the cementitious matrix is pulled along its axis, and the load versus displacement relation is measured to determine the bond capacity as well as parameters governing the bond. In the literature, several testing configurations have been employed. Windisch [23] performed the pull-out test according to recommendations of RILEM/CEB/FIP Committee. In this test, the pulling force is balanced by compression on the surface where the bar is coming out. The generated compressive zone near the surface may affect the bond capacity. Chana [5] conducted the 'eccentric pull-out test' to demonstrate the realistic situation (pull-out under bending) of tensile reinforcement in concrete beam. Although this configuration is close to the real situation, the effect of bending on the pull-out bar is sensitive to the anchorage length of embedded bar. In this investigation, the direct tension pullout bond test (DTP-BT) suggested by Cheung and Leung [6] is employed.

A rectangular HSFRCC plate with embedded GFRP bars was employed for the pull-out test. The GFRP employed in our work is the Reno Composite Material System (Electric Insulator Co. Ltd., Taiwan). The properties of GFRP rebar provided by manufacturer are summarized in Table 1. The mix proportion of HSFRCC is provided in the second column of Table 2. The compressive strength of the HSFRCC is obtained from the test of 100 mm cube, and the average value is 150 MPa. Its flexural strength is obtained from four point bending test on 75 × 75 × 300 mm beam. The average result is 20 MPa. All specimens were tested after 28 day curing. To represent the joint of PDCC formwork, the size of the HSFRCC plates was designed to be 150 × 400 × 30 mm (width × length × depth), with the depth being the same as that for a typical

Table 1 Properties of GFRP Reinforcement

Diameter (mm)	Ultimate tensile strength (MPa)	Tensile modulus of elasticity (GPa)
6	825	40.8

Table 2 Mix proportion of the PDCC and HSFRCC

Material	PDCC (ratio)	HSFRCC (kg/m^3)
Fly ash	0.8	247
Cement	0.18	1,010
Silica fume	0.02	112
Silica sand[a]	0.2	874
Water	0.22	260
Superplasticizer[b]	0.0051	11.5
Fiber (2 %)	PVA	Steel

[a] Single size sand 53–300 μm for PDCC and graded silica sand 53–1,180 μm

[b] Suitable SP are used

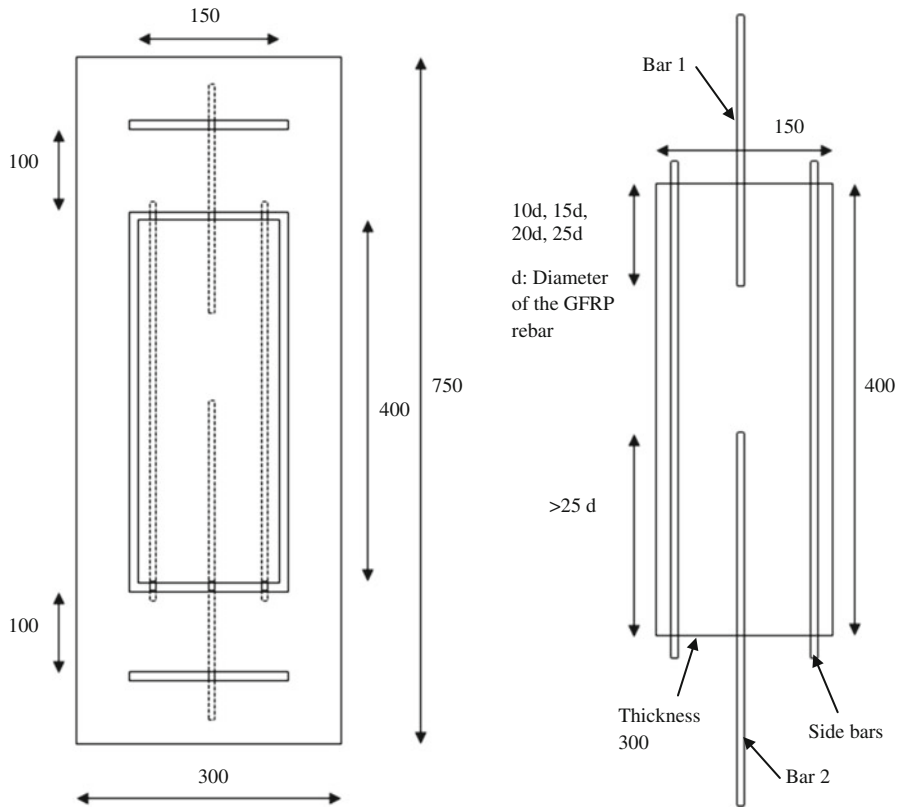

(a) Wooden Formwork **(b)** Specimens

Fig. 2 Preparation for direct pull-out test (units all in mm)

PDCC formwork element. To make the specimens, a wooden formwork as shown in Fig. 2a was designed. GFRP bars were placed in proper position inside the wooden formwork before the casting of HSFRCC. The configuration of test specimen is shown in Fig. 2b. Bar 1 represents the tested GFRP bar with varied embedded length. To ensure the occurrence of failure at Bar 1, a longer GFRP bar (>25*d*, Bar 2), aligned along the same line as Bar 1, was embedded on the other side of the specimen. To prevent tensile failure of the HSFRCC plate, side bars were inserted near the edges along the longitudinal direction. It should be noted that side bars are only needed for the test specimen. In the real situation, the lapping embedded bars can prevent the tensile failure of HSFRCC by themselves.

In order to provide sufficient data for the extraction of interfacial parameters and verification of the theoretical bond model, four groups of specimens with different GFRP embedded lengths of 10*d*, 15*d*, 20*d* and 25*d* (where *d* is the diameter of the GFRP bars) were prepared. The range of embedded length was chosen according to the minimum lap length of steel reinforcement which is equal to 15*d* [4]. As the GFRP bars employed in this project was 6 mm in diameter, the embedded lengths were 60, 90, 120 and 150 mm accordingly (Fig. 2b). Three specimens were prepared for each case. After casting, the specimens were cured in an environmental room (at 98 % relative humidity and 25 °C) for a total of 28 days before preparation for testing.

2.2 Pull-out testing

To perform pull-out testing, the aligned GFRP bars coming out from both ends of the sample are held inside the hydraulic grips of an universal testing machine. As GFRP is very brittle, the ends of the GFRP rod need to be specially designed to avoid gripping failure. In our work, three pieces of bi-directional GFRP fabric was wrapped on the GFRP bars with epoxy resin as the adhesive agent (Fig. 3a). Bi-directional fabric is used instead of sheets with aligned fibers because the former has a much higher shear strength which is important for

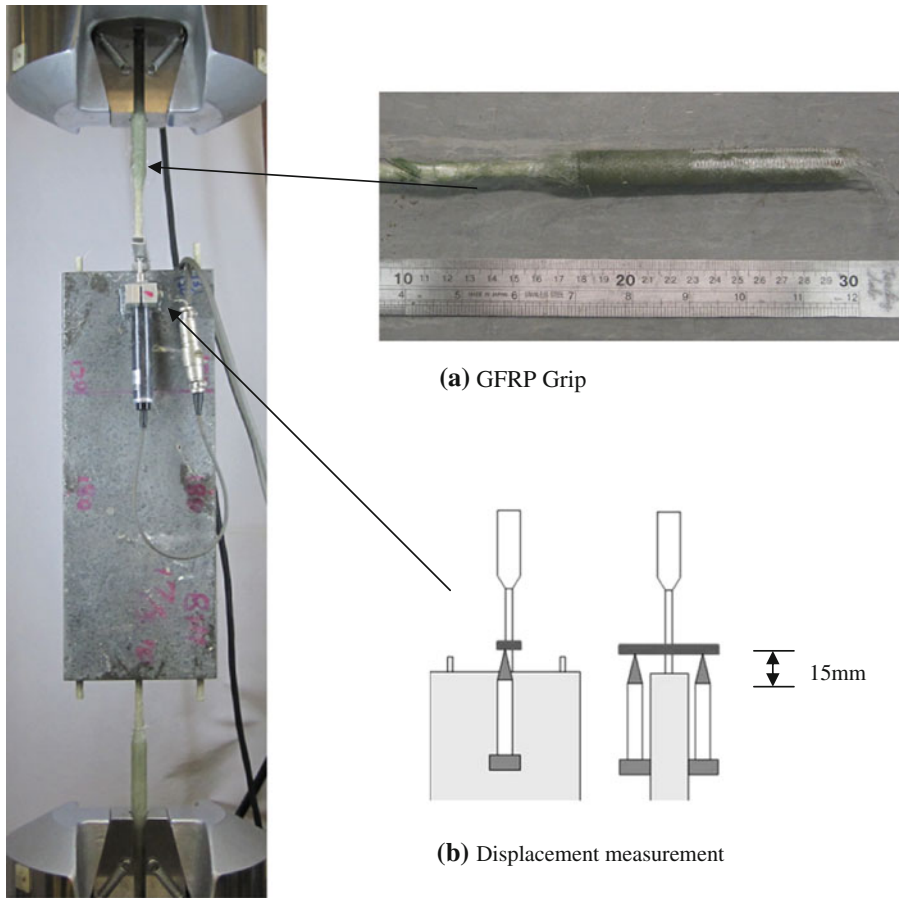

(a) GFRP Grip

(b) Displacement measurement

Fig. 3 Direct pull-out test set-up

preventing gripping failure. To show the effectiveness of this approach, direct tensile test has been performed on GFRP bars with wrapped fabric at the ends. In these tests, tensile rupture of the bar was found to occur away from the grip at a load value similar to that reported by the manufacturer. After ensuring the gripping failure could be avoided, the pull-out test was performed with the testing set up in Fig. 3b.

To measure displacement during the direct pull-out test, an aluminum plate (serving as a reference point for the measurement of displacement during testing) was glued on the exposed GFRP bar of the specimen with hot melt adhesive. The plate was placed away from the GFRP grip and at a distance of 15 mm away from the edge of HSFRCC plate. Two linear variable differential transformers (LVDT) were placed vertically to measure the displacement of GFRP Bar 1 (Fig. 3c). During the test, displacement control was applied at a loading rate of 0.1 mm/min.

2.3 Test results and discussions

The ultimate failure load for all four groups of specimens is summarized in Table 3, together with the failure modes. It should be pointed out that cracking and peel-off of HSFRCC were observed near the junctions of GFRP bars and HSFRCC plates. Possible reason for the phenomenon was that the HSFRCC plates were not thick enough to provide enough confinement to resist the micro-cracking around the GFRP bar. The chosen thickness is consistent with that for common PDCC formwork elements. However, in real joint construction, peeling-off of HSFRCC may occur to a smaller extent because the cast concrete on one side of the formwork will limit the peeling to the other side only. The typical force versus displacement curves of all groups are illustrated in Fig. 4. For the group with 150 mm embedded GFRP bar, the failure mode was observed to be GFRP bar rupture. The failure occurred on either

Table 3 Summary of experimental results of the specimens

Specimen batch	Embedded length (mm)	Average measured ultimate tensile load (kN)	Failure mode
HSFRCC/GFRP(60)	60 (10*d*)	13.89	Pull-out of GFRP bar
HSFRCC/GFRP(90)	90 (15*d*)	17.60	Pull-out of GFRP bar
HSFRCC/GFRP(120)	120 (20*d*)	22.88	Rupture/pull-out of GFRP bar
HSFRCC/GFRP(150)	150 (25*d*)	22.99	Rupture of GFRP bar

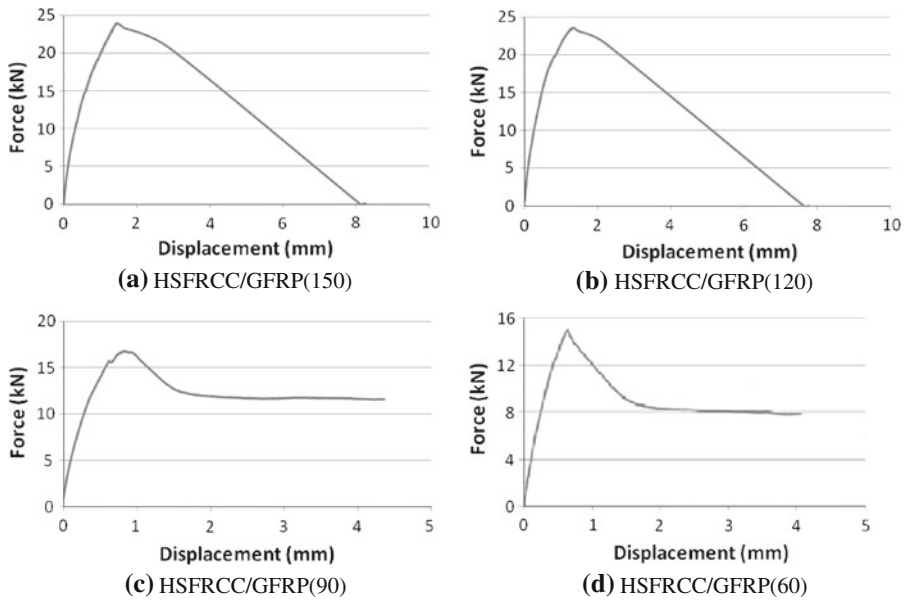

Fig. 4 Typical force against displacement curve

the shorter bar of interest (Bar 1) or the longer one (Bar 2). The average rupture strength of 22.99 kN is similar to theoretical value of 23.32 kN calculated from the GFRP strength and diameter given in Table 1. For the group with 120 mm embedded GFRP bar, the ultimate load was within the same range as that of the last group with 150 mm embedded length. However, two out of the three specimens were observed to fail by bar rupture while the other one showed pull-out failure of the rebar. Based on the observation from the data and specimens, it was suggested that the critical embedded length could be around 120 mm (20*d*) as the pull-out load capacity is similar to the rupture load at this embedded length. For the groups with 90 and 60 mm embedded GFRP bar, pull-out failure of the shorter GFRP bar (Bar 1) occurred instead and lower values of ultimate tensile load were measured. Based on the pull-out failure of GFRP bars, it can be concluded that the critical embedded length for GFRP rupture had not been reached at 90 mm (15*d*).

3 Data analysis for determination of interfacial parameters

In order to connect two permanent formwork elements, load has to be transferred from one element to another through an effective joint. Therefore, its width has to be determined first. The joint width is controlled by the lap length of the reinforcement protruded from the permanent formwork. For the proposed joining method, the relationship between the embedded length of GFRP in HSFRCC and its load carrying capacity has to be determined. To find this relation, the

(a) GFRP rupture **(b)** GFRP Pull-out

Fig. 5 No spalling or large cracks can be observed

governing parameters to predict the loading capacity should be identified first. According to Fig. 5, no significant damage (such as splitting cracks or major spalling) was observed in specimens failed by either GFRP pullout or rupture. This is certainly very different from conventional pull-out test performed on steel bars embedded in normal concrete specimens with small cover, where severe splitting and/or spalling can be found. This should be due to the high strength and toughness of HSFRCC which effectively controls the propagation and opening of cracks. Since there is only limited damage in the concrete around the bar, one may adopt a simple model that assumes the failure to localize along the interface between GFRP and HSFRCC matrix. The loading capacity is then governed by the interfacial parameters at the HSFRCC/GFRP interface. These parameters can be obtained with the help of a theoretical model developed by Stang et al. [20] for interfacial debonding and pull-out of single fiber from an elastic matrix. The applicability of the model to the determination of interfacial parameters has been verified in Li et al. [13].

For an embedded GFRP rebar under pulling force, the geometry (debonding length '*a*' and embedded length *L*) and the three major interfacial parameters (*k*, τ_y and τ_f) are illustrated in Fig. 6. The model in Stang et al. [20] is based on the assumption that interfacial debonding starts to occur once the interfacial bond strength (τ_y) is reached. Before debonding, the interfacial shear stress increases linearly with fiber/matrix

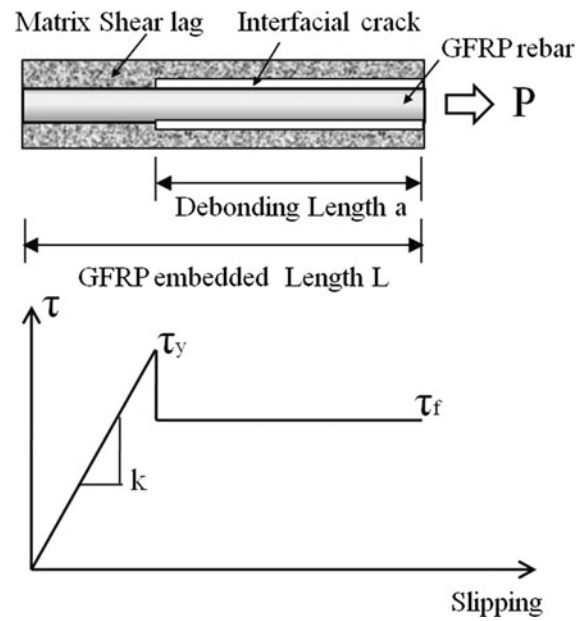

Fig. 6 Pull out problem with a stress versus slipping curve

relative displacement and the proportionality constant is shear stiffness *k*. After debonding, the interfacial stress will drop immediately to the interfacial friction (τ_f). The Interfacial friction τ_f is caused by the undulating surface of GFRP rebar and surrounding matrix and is assumed in our work to stay constant on further interfacial sliding. In the model, three related parameters were introduced: the maximum shear force per unit length q_y, frictional shear force per unit length q_f and interfacial stiffness parameter ω, where

$$q_y = 2\pi r\tau_y \quad (1)$$

$$q_f = 2\pi r\tau_f \quad (2)$$

$$\omega = \sqrt{\frac{k}{E_f A}} \quad (3)$$

Assuming the concrete to be rigid and considering the equilibrium between axial force in the GFRP and shear force along the GFRP/concrete interface, two differential equations can be derived for the axial displacement of the bar for the bonded part ($0 < x < L - a$) and the debonded part ($L - a < x < L$). Using appropriate boundary conditions, the relations between applied loading, debonded length (a) and displacement at the loading point can be derived.

To illustrate the determination of interfacial parameters, the experimental curve of a specimen with 90 mm GFRP embedment length (Fig. 4c) is taken as an example. It is first simplified into a multi-linear load versus displacement curve (Fig. 7) for the identification of key points in the curve. All the points are based on the average values of three tests in this group. In the post-peak region beyond point C, the loading is dropping slowly in a linear manner. The interface is then governed by friction alone. q_f can then be calculated from the load P at point C and the remaining embedded length of the GFRP bar, from:

$$q_f = \frac{P}{U} = \frac{12.4}{90 - 1.6} = 0.14\,\text{kN/mm} \quad (4)$$

where U is the displacement at the pulled end of embedded GFRP.

According to the model of Stang et al. [20], when debonding just starts to occur (i.e., at the end of the elastic stage), U is related to the initial debonding load (P_y) through:

$$U = \frac{P_y}{E_f A_\omega}\coth(\omega L) \quad (5)$$

Initial debonding is taken to occur at point A in Fig. 7, where the corresponding curve in Fig. 4c starts to deviate significantly from the initial linear behavior. At this point, the measured displacement (δ_{total}) consists of two parts, the displacement (U) of GFRP bar at the edge of the HSFRCC plate and the elongation of the bar for the 15 mm length between the glued aluminum plate and the edge of HSFRCC plate. With P_y obtained at point A, U is determined from:

$$\delta_{total} = \frac{P_y \times 1}{E_a \times A} + U \quad (6)$$

For the data shown in Fig. 7, $P_y = 12$ kN and $\delta_{total} = 0.4$ mm. Also, with properties of the GFRP bar, $A = 28.3$ mm^2 and $E_a = 40.8$ GPa, the value of U is found to be 0.24 mm, ω can be calculated by substituting $L = 90$ mm into Eq. 5. The value of ω is found to be 0.043. After the onset of interfacial debonding, the load for a particular debonded length (a) can be calculated from the interfacial parameters through Eq. 7 (derived in Stang et al. [20]):

$$P = q_f a + \frac{q_y}{\omega}\tanh[\omega(L - a)] \quad (7)$$

To determine q_y, an iterative procedure is employed. A value of q_y is first assumed and used for the calculation of P in Eq. 7. The debonded length a is varied until a maximum value is reached. There will always be a maximum value for P if q_y is greater than q_f, which is one of the basic assumptions of the model. This maximum value is compared to the peak load measured in the pull-out test. Depending on whether the calculated value is larger or smaller, a smaller or larger q_y will be employed in the next iteration. The procedure is repeated until the peak load calculated from the model is consistent with the test result. The corresponding value of q_y is taken as the actual interfacial strength. Using the corresponding result in Fig. 7, q_y was found to be 0.48 kN/mm.

After determining the interfacial parameters (q_y, q_f and ω) from one test, the pull-out force P_{max} for any embedded length can be calculated. In Table 4, the calculated results for all tested embedded lengths are

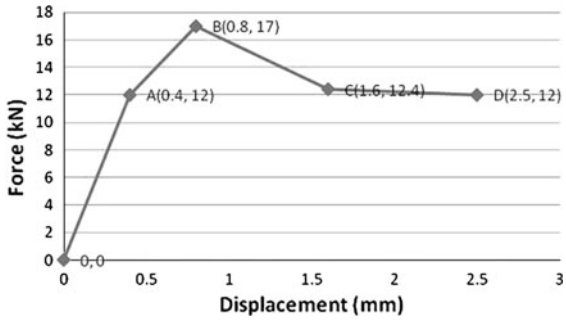

Fig. 7 Simplified curve for group with 90 mm embedded GFRP bar

Table 4 Comparison between experimental and calculated values

Specimen	Ultimate tensile load (experimental) (kN)	Tensile load (numerical analysis) (kN)	Percentage error
HSFRCC/ GFRP(60)	13.89	13.85	−0.3
HSFRCC/ GFRP(90)	17.60	18.06	2.6
HSFRCC/ GFRP(120)	22.88	22.27	−2.7
HSFRCC/ GFRP(150)	22.99	26.47	15.1

compared to the experimental data. Except for the group with 150 mm embedded length, the values generated from the numerical model are in close agreement to the experimental results (with the percentage error of less than 3 %). This observation indicates that the simple model of Stang et al. [20] is suitable for determining the relation between the maximum pull-out force for GFRP bar and its embedded length. When the embedded length is 150 mm, failure occurs by rupture instead. As expected, the calculated debonded load is higher than the failure load. To take GFRP rupture into consideration, the pull-out capacity is bounded by the ultimate tensile load capacity of GFRP rebar, which is 23.32 kN. According to the pull-out capacity as well as the failure mode of GFRP, it is safe to say that, with a joint width larger than 126 mm (21d), there is sufficient stress transfer to reach the rupture load of the GFRP bar.

4 Four point bending test

4.1 Specimen preparation

To demonstrate the proposed joining method, PDCC formwork with embedded GFRP were first cast. The mix proportion of PDCC is shown in the first column of Table 2 and polyvinyl alcohol (PVA) fibers was used to make the PDCC and. To ensure uniform fiber distribution and to control the toughness of the matrix, fine silica sand is used in the matrix and no coarse aggregates are incorporated. In this paper, 80 % by weight of the cement was replaced by fly ash. As fly ash is a waste material, the use of a large amount of fly ash in the PDCC can be considered a 'green' approach [25].

In this study, channel-shaped permanent formwork elements were prepared with the use of wooden molds. Before casting of PDCC, GFRP rods were inserted through holds in the end plates of the mold and supported intermittently with spacers. Since the selected PDCC had high workability, the formwork element was fabricated without internal vibration or tampering. When the material was still fresh, lateral grooves were introduced on the surface. To cast the channel-shaped element, a wood mold as shown in Fig. 8 was employed. The mold is assembled of three planks connected by two hinges. Its inner surface is lined with a rubber sheet so the joints (at the hinged locations) are properly sealed to prevent water and fine particles from leaking out. There is a wooden strip placed along each of the two side planks to maintain a certain thickness of PDCC during casting. At the middle plank, an additional pair of strips (called the thickness adjuster) was placed to allow the casting of PDCC to a higher thickness than that on the sides. After initial setting, the thickness adjuster is removed. Since the concrete is sufficiently stiff, the middle part will remain higher than the sides. The two side planks are folded up to form the channel formwork. In our tests, the thickness at the bottom part of the channel formwork was 30 mm to provide a proper cover to the GFRP rods inside. The two legs (formed by folding up of PDCC) were 20 mm in thickness.

To study the effectiveness of the joining method, two groups of beam members were prepared for four point bending test. In group BC (control), a monolithic formwork was employed. In group BJ, the formwork was made by two PDCC elements held together with the HSFRCC joint. The mix proportion of HSFRCC in group BJ is the same as that in the direct pull out test. The mechanical properties of PDCC and HSFRCC are provided in Table 5. A spacing of 1.5d (9 mm) was kept between two GFRP bars (Fig. 9). According to the result in pull out test, the embedded length of 126 mm (21d) is sufficient to cause the rupture failure of GFRP rebar. Therefore, to provide the sufficient load capacity, the lap length of 130 mm (>126 mm) between GFRP rebar was provided in the test. In normal reinforced concrete members, the lap length is often longer than the anchorage length for bar failure to occur in the pull-out test. This is because the high stresses between adjacent bars can result in severe

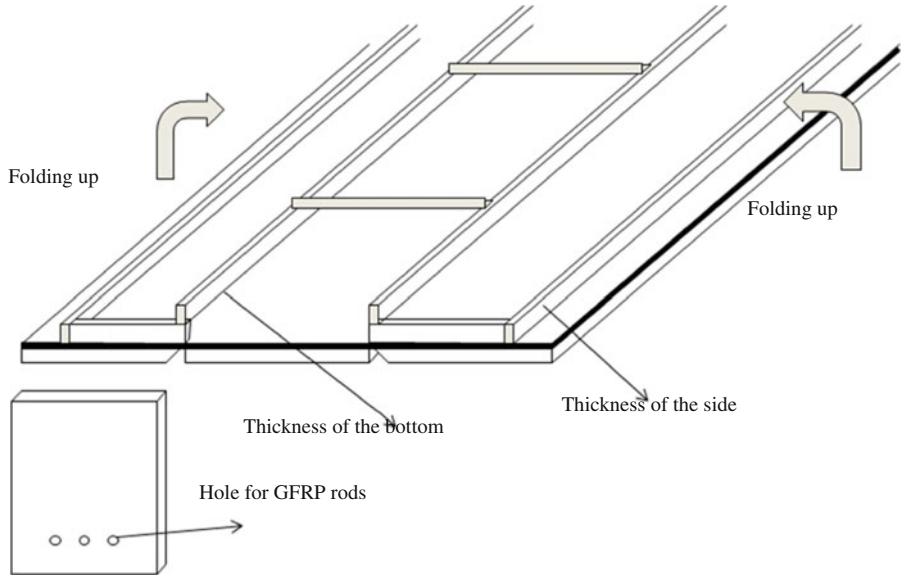

Fig. 8 Wooden mould for U-shape formwork

Table 5 Properties of PDCC and HSFRCC

Type	Compressive strength (MPa)	Tensile strength (MPa)	E (GPa)
PDCC	33	3–5	18
HSFRCC	150	9	38

cracking and splitting that reduces the load transfer capability. In our case, due to the very high strength and toughness of the HSFRCC, limited damage occurs inside the concrete. The "interactive" effect between adjacent bars can therefore be neglected. This assumption is shown to be reasonable by the experimental results (which will be described in detail later) which do not show GFRP debonding up to the failure load.

To prevent bond failure at the PDCC/HSFRCC interface, each formwork element was prepared with a zig-zag edge by placing wooden blocks at the end of the mold. Taking the zigzag edge into consideration, the whole joining area with 150 mm length was reserved for casting HSFRCC joint (Fig. 9). The difference between the two groups of beams was hence the absence or presence of the joint. Since the whole joining area was designed under a constant moment, the HSFRCC joint thus is under pure tension

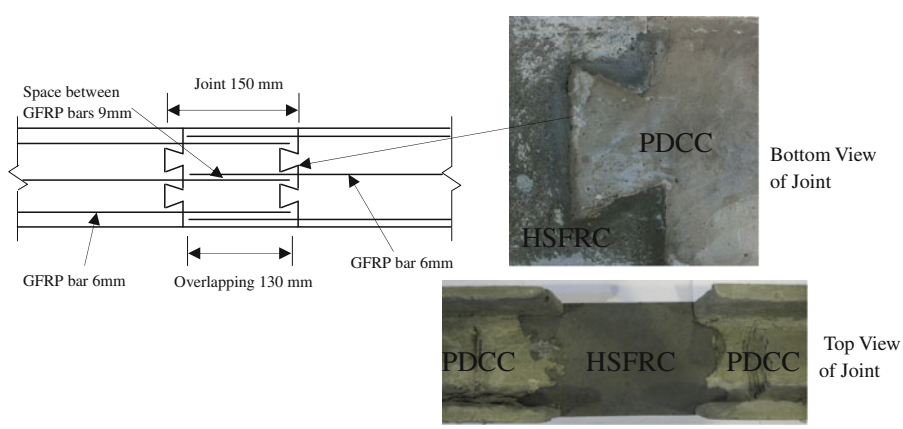

Fig. 9 Configuration of GFRP rebar in joint

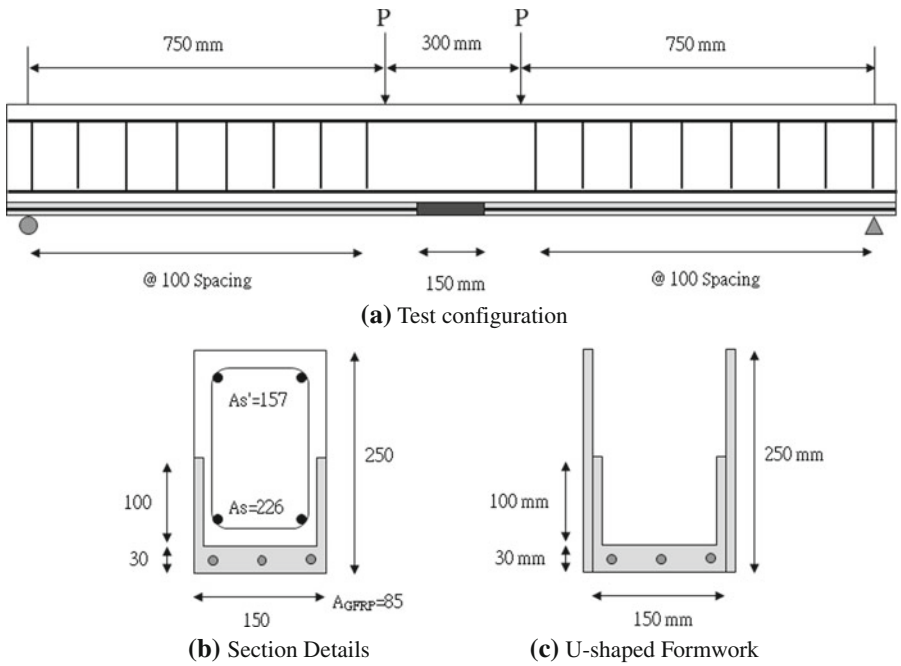

(a) Test configuration

(b) Section Details **(c)** U-shaped Formwork

Fig. 10 Test configurations and specimen details (units all in mm)

on the bottom of test beam. Although the channel-shaped PDCC formwork is used in our test, the HSFRCC joint is only made on the bottom to verify its feasibility. If there is a need to prevent water/chemicals from getting in from the sides of the concrete above the joint, additional PDCC plates can be added.

After 28 day curing of the PDCC, the channel shaped formwork was placed in a rectangular wooden mould with both ends sealed by wooden plate and the test beam was then cast in this mould. The tested beam is 2 m long (Fig. 10a). The cross section of beam member was 250 mm in depth (including the permanent formwork) and 150 mm in width. The design details of the steel reinforcements are shown in Fig. 10b and the reinforcement ratio was the same (around 1 %) in all the tested beams. The beams were all under-reinforced with high yield steel bars (460 MPa): two 12 mm tension bars, two 10 mm compression bars, and 8 mm steel stirrups at 100 mm spacing. All beams were designed for flexural failure well before failure in shear. Concrete with compressive strength of 45 MPa was employed to make the beams (by 100 mm cube test). After concrete casting, all the beams were cured for 28 days before testing under four point bending. For each group, three specimens were prepared and tested.

A comment should be made on the use of channel shaped formwork in our experiments. In practice, the sides of the member should also be covered by the permanent formwork. A simply example, for the casting of a rectangular beam, is given in Fig. 10c. Two rectangular plate formwork elements are glued to the sides to make a U-shaped formwork for the beam. Indeed, more complicated shapes can be made by combinations of channel-shaped, L-shaped (prepared in the similar way as the channel, but only one side is folded up) and plate formwork elements. In our experiments, for simplicity, the side plates are not added. We believe this will not change our conclusions about the design of the joint and its load capacity, as the addition of side plates will not degrade the joint. The addition of side plates to the channel-shaped formwork also increases the flexural stiffness. During the casting of concrete, a stiffer formwork will allow a larger spacing between the falsework supports. A simple example illustrating the calculation of support spacing for the permanent formwork can be found in Leung and Cao [8].

In practical applications, the formwork elements will be pre-casted (assumed to be fully cured) and connected on-site. To simulate the real condition, all PDCC formwork elements in our test were cured for 28 days before casting the joint. The joint is prepared

Fig. 11 Verification of joining method in the practical application

by the HSFRCC. To further simulate the real condition, a person with 70 kg (around 700 N) weight was asked to stand on the joint with two point supports (Fig. 11). This can be considered the most critical loading condition of the formwork during the construction stage. The result verifies that HSFRCC joint can provide sufficient load capacity for a worker walking and/or standing on the plain PDCC formwork in site.

4.2 Test setup

The testing configurations for all the beams are shown in Fig. 10a. In the test, the beam member was set up on the 500 kN Material Testing System (MTS) with loading span L of 1,800 mm. Four-point loading was applied with equal force acting at distance of 750 mm from each support. A linear variable differential transformers (LVDT) was placed at the bottom of the beam to measure the middle deflection. The test was conducted under displacement control at the loading rate of 0.5 mm/min.

4.3 Test results and discussion

The results of four point bending test are summarized in Table 6. The typical load versus central deflection curves of group BC and BJ are shown in Fig. 12. The average ultimate load of group BC is 115 kN and the average ultimate load is 110 kN for group BJ. Comparing the test results of the monolithic and joining members in terms of ultimate load capacity, the joining members can provide almost the same load (110/115 = 95.7 %) as the case without the joint. With this result, the joint is unlikely to affect the loading capacity under practical situations, as it will normally be placed at a location with low bending moment. During the tests in both group BC and group BJ, fine multiple cracks were found to form along the specimen when the loading was increased. When the

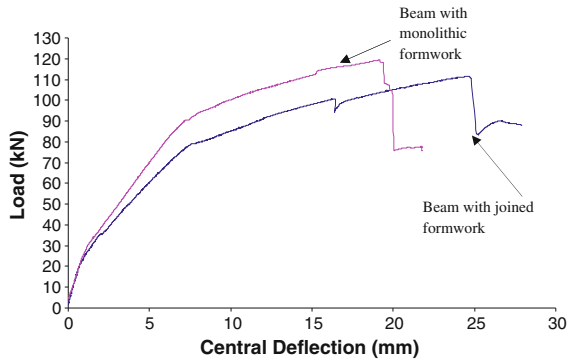

Fig. 12 Test result for four point bending

Table 6 Result of four point bending test

Series	Specimens	Designed flexural capacity (kNm)	Designed applied load (kN)	Test moment (kNm)	Test load (kN)
BC	1	35.4	94.5	43.1	114.9
	2			42.8	114.1
	3			43.7	116.5
	Average			43.2	115.2
BJ	1	35.4	94.5	41.3	110.1
	2			40.7	108.5
	3			41.8	111.4
	Average			41.3	110

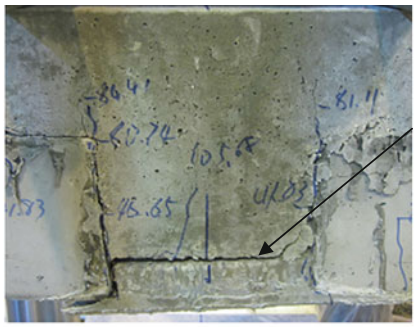

(a) Debonding on the boundary

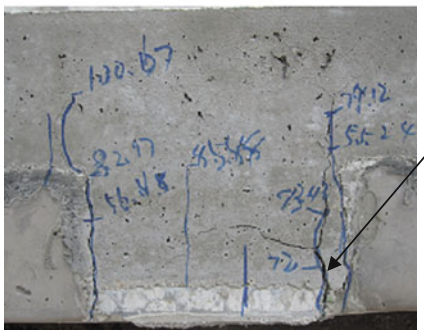

(b) Debonding in the concrete

Fig. 13 Failure mode for Group BJ

load approached 73–76 % of ultimate load (88 kN for group BC and 80 for group BJ), a major crack started to localize. The members of the control group BC finally failed in flexure with a major localized crack under the loading point. The group BJ was failed by GFRP rupture instead. According to Fig. 13, debonding was observed before the final failure and it mainly occurred at two different locations: (i) the boundary between HSFRCC joint and concrete (Fig. 13a) if the bonding is relatively weak, and (ii) in the concrete at the level of steel reinforcement if the bonding is strong (Fig. 13b). However, it is interesting to see that both kinds of debonding failure occurred at similar loading (100 kN) and exhibited similar load versus displacement behavior (Fig. 14). It should also be pointed out that GFRP debonding and pull-out has not been observed in our tests, indicating that the lap length is sufficient.

For the member with joined permanent formwork, different stages of crack growth are summarized and illustrated in Figs. 15 and 16. At stage 1, some fine cracks first occurred below the loading point. With load increase, the crack below the loading point started to propagate and other cracks started to form along the specimen. When the crack started to initiate at the interface of joint at stage 2, the stiffness started to decrease. The crack started to propagate on the interface of joint at stage 3. When the debonding occurred at the interface of joint (stage 4), a small drop was observed. This drop should be due to the debonding of interface between PDCC formwork and HSFRCC joint. The force taken by the formwork thus was mainly taken by GFRP reinforcement. When the final failure approached at stage 5, with the

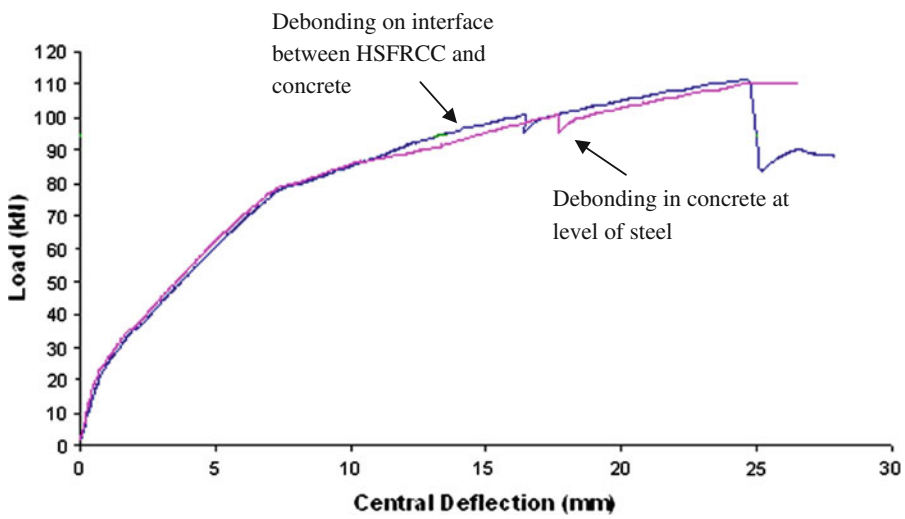

Fig. 14 Comparison between two different debonding patterns

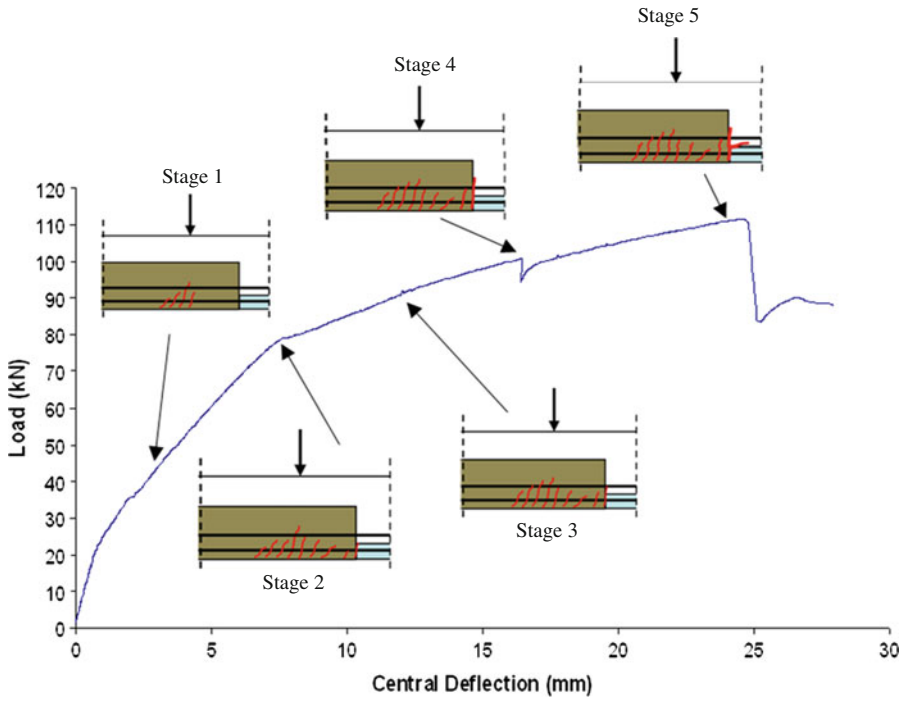

Fig. 15 Stages of crack development

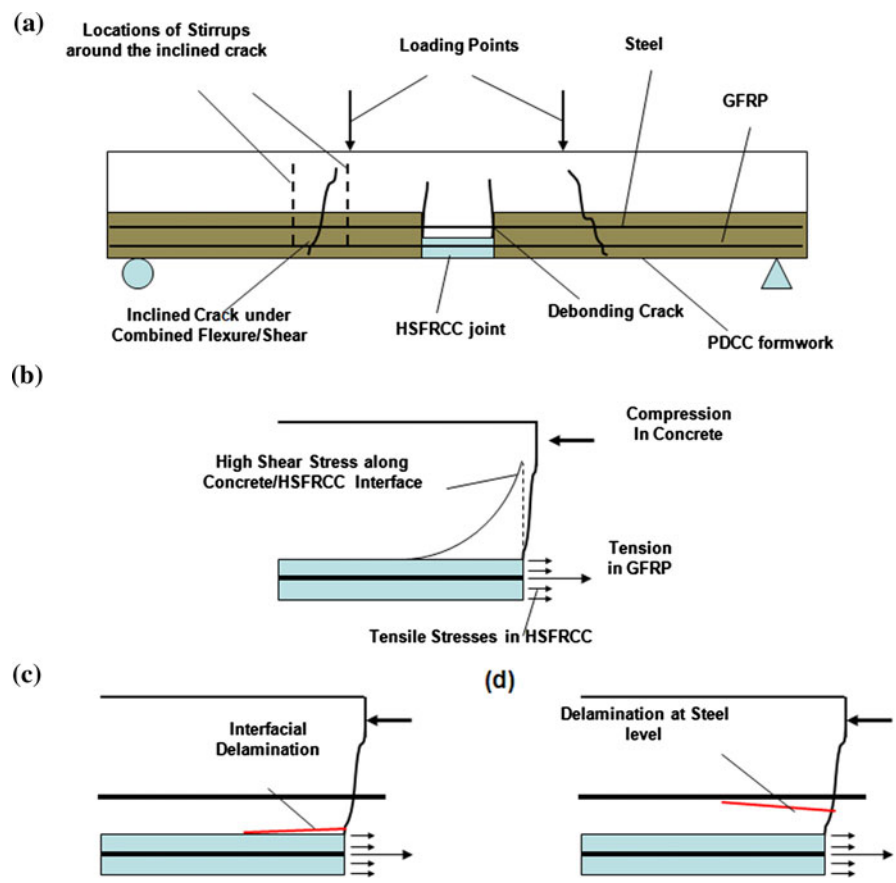

Fig. 16 Delamination of in the joint. **a** Major cracks along the member, **b** development of shear stresses along the concrete/HSFRCC interface, **c**, **d** interfacial delamination

increase of loading in the GFRP bar, the shear stress along the interface was increased. Since the material of joint (HSFRCC) had higher stiffness than concrete, high shear stress was introduced at concrete/HSFRCC interface (Fig. 16). The crack on the connection could then propagate in two ways: (1) If the bond between HSFRCC and concrete is weak, the crack may run along the concrete/HSFRCC interface (Figs. 13a, 16c); (2) If the bond is strong, the crack may go up to the level of steel reinforcement and propagate along the bottom of the reinforcements (Figs. 13b, 16d) since the bottom of the steel reinforcements can be considered to form a weak horizontal plan in the member. When the GFRP rebar reach its ultimate tensile strength, the rupture of GFRP rebar was observed.

In the tests, the members with monolithic formwork appeared to fail in flexure. For the members with joined formwork, failure was initiated by debonding (at the HSFRCC/concrete interface or at the steel level) and ended by GFRP rupture. Fine multiple cracks could still form along the specimen and the opening of HPFRCC/PDCC interface at the joint only started to occur after the load reached 73 % of ultimate load (80 kN). It should be noted that the joint was placed at the location with the maximum moment in our test to simulate the worst scenario and to obtain the ultimate loading capacity. However, in practice, the worst scenario would rarely happen because the joint would most likely be placed at a location with much lower moment. Therefore, if we adopt the conventional approach to design the beam, the joining method proposed in this study is acceptable as it is able to maintain a load capacity higher than the service load, which is normally less than one-half of the ultimate.

5 Conclusions

In this paper, a joining method for permanent formwork elements, which involve the embedment of extended GFRP reinforcements in HSFRCC matrix, is proposed and studied. The direct pull-out test was carried out on specimens made with HSFRCC joint material and GFRP reinforcement. Interfacial parameters governing the bonding behavior were first extracted from the experimental data according to a debonding model. After the interfacial parameters were successfully obtained, the required embedment length of GFRP bars in the joint can be predicted. To fully utilize the capacity of GFRP rebar, the rupture failure has to be ensured and the recommended length should be greater than about $21d$ (i.e. 126 mm for 6 mm-diameter GFRP bars). To verify the joining method, the four point bending test was carried out on beams made with joined permanent formwork elements. Following the results from the bond test, the lapping length of GFRP bars inside the joint was 130 mm. In the test, pull-out failure of the GFRP was not observed. In the presence of the joint, the beam can attain over 95 % of the ultimate loading for the beam made with a single formwork element. With this result, the joint is unlikely to affect the loading capacity under practical situations, as it will normally be placed at a location with much lower moment. The feasibility of the proposed joining method for practical applications is hence verified.

Acknowledgments Financial support of the work by the Hong Kong Research Grant Council, under CERG UST615508, is gratefully acknowledged.

References

1. Bentur A, Diamond S, Berke N (1997) Steel corrosion in concrete: fundamentals and civil engineering practice, 2nd edn. E & FN Spon, New York
2. Birelli G, Cadoret G, Dutaillor F, Thibaud T (1998) A new, very high performance concrete. In: International symposium on high-performance and reactive powder concretes, vol 3, pp 177–201
3. Brameshuber W, Brockman J, Rossler G (2001) Textile reinforced concrete for formwork elements—investigation of structural behaviour. In: Burgoyne C (ed) Proceedings of FRPRCS-5, pp 1019–1026
4. BS 8110-1 (1997) British standard: structural use of concret. Part 1: code of practice for design and construction
5. Chana P (1990) A test method to establish a realistic bond stress. Mag Concr Res 24(151):83–90
6. Cheung AKF, Leung CKY (2011) Effective joining of precast concrete slabs with self-compacting HSFRCC. Jpn Concr Inst J Adv Concr Technol 9(1):1–9
7. Jensen BC et al (1995) Connections in precast buildings using ultra high-strength fibre reinforced concrete. In: Nordic symposium on modern design of concrete structures, Aalborg University, Denmark
8. Leung CKY, Cao Q (2010) Development of pseudo-ductile permanent formwork for durable concrete structures. RILEM Mater Struct 43(7):993–1007
9. Leung CKY (1996) Design criteria for pseudo-ductile fiber composites. ASCE J Eng Mech 122(1):10–18
10. Li VC (1993) From micromechanics to structural engineering—the design of cementitious composites for civil

engineering applications. JSCE J Struct Mech Earthquake Eng 10(2):37–48
11. Li VC, Leung CKY (1992) Steady state and multiple cracking of short random fiber composites. ASCE J Eng Mech 188(11):2246–2264
12. Miyazato S, Hiraishi Y (2004) Transport properties and steel corrosion in ductile fiber reinforced cement composites. In: Proceedings of 11th international conference on fracture, Paper No. 4484, CD ROM
13. Li Z, Mobasher B, Shah SP (1991) Characterization of interfacial properties in fiber-reinforced cementitious composites. J Am Ceram Soc 74(9):2156–2164
14. Ma J, Dietz J (2002) Ultra high performance self compacting concrete. Lacer 7:33–42
15. Naaman AE (2003) Strain hardening and deflection hardening fiber reinforced cement composites. In: Naaman AE, Reinhardt HW (eds) High performance fiber reinforced cement composites (HPFRCC-4). RILEM Publications, Pro 30, pp 95–113
16. Ogawa A, Hitomi Y, Hoshiro H (2006) PVA-fiber reinforced high performance cement board. In: Fischer G, Li VC (eds) Proceedings of international RILEM workshop on HPFRCC in structural applications, pp 243–251
17. Parameswaran VS, Krishnamoorthy TS, Balasubramanian K (1990) Behaviour of high volume fibre cement mortar in flexure. Cement Concr Compos 12:293–301
18. Richard P, Cheyrezy M (1995) Composition of reactive powder concretes. Cem Concr Res 25(7):1501–1511
19. Shioya T et al (1997) Pre-cast concrete joint using steel fiber reinforced high strength mortar and/or H-beam. Proc Jpn Concr Inst 19(2):1305–1310
20. Stang H, Li Z, Shah SP (1990) Pull-out problem: stress versus fracture mechanical approach. Eng Mech ASCE 116(10):2136–2150
21. Takewaka K, Yamaguchi T, Maeda S (2003) Simulation models for deterioration of concrete structures due to chloride attack. J Adv Concr Technol 1(2):139–146
22. Wang K, Jansen D, Shah S, Karr A (1997) Permeability study of cracked concrete. Cem Concr Res 27(3):381–393
23. Windisch A (1985) A modified pull-out test and new evaluation methods for a more real local bond-slip relationship. Mater Struct 18(3):181–184
24. Yamada K, Saijo R, Furumura T, Tanaka S (2006) Application of extrusion molded DFRCC to permanent form. In: Fischer G, Li VC (eds) Proceedings of international RILEM workshop on HPFRCC in structural applications, pp 253–260
25. Yang EH, Yang YZ, Li VC (2007) Use of high volumes of fly ash to improve ECC mechanical properties and material greenness. ACI Materials J 104(6):620–628
26. Yu C, Leung CKY, Cao Q (2010) Behavior of concrete members constructed with SHCC/GFRP permanent formwork. In: Proceedings of 7th international conference on fracture mechanics of concrete and concrete structures, CD ROM
27. Yudenfreund M, Odler I, Brunauer S (1972) Hardened Portland cement pastes of low porosity, I. Materials and experimental methods. Cem Concr Res 2(3):313–330